Mechanical degradation and viscous dissipation in B_2O_3

John Kieffer
Department of Materials Science and Engineering, University of Illinois, Urbana, Illinois 61801
(Received 12 January 1994)

The Brillouin light scattering technique was used to determine the complex mechanical modulus, which describes the dynamic response of molecular structures, for B_2O_3 and binary alkali borate. The effects of temperature, alkali concentration, oxygen and water vapor partial pressures on the structural developments and on the thermal activation of dissipative processes were examined. The glass transition in these systems is characterized by a discontinuity in the temperature dependence of the elastic component of this modulus. Above T_g, the elastic modulus decreases with a faster rate, the higher the alkali concentration. The complete structural evolution from a room temperature glass to a liquid near the boiling point was found to involve several distinct mechanisms, which become gradually activated with increasing temperature. By using a mechanical relaxation formalism, the activation energies and preexponential time constants describing the mechanical degradation, as well as the molecular rearrangements associated with each mechanism were determined. For a given system, the initial network degradation is characterized by the smallest activation energy. The motion involved in this process is that of boron atoms oscillating between triangular and tetrahedral coordination, upon exchanging one of their oxygen neighbors. During this phase boroxol rings open, without the formation of nonbridging oxygens. At intermediate temperatures the motion of alkali cations between network segments is activated, and at very high temperatures complete network disintegration takes place, leaving ionic species whose motion occurs by complete dissociation from their immediate neighbors.

I. INTRODUCTION

As the network forming component in glasses, such as superionic solid electrolytes or materials with high thermal shock resistance, boron oxide has been given considerable attention. The structure and properties of pure boron oxide, as well as of multicomponent borates, have been the subject of numerous investigations. The results from x-ray diffraction,[1] Raman scattering,[2,3] and NMR (Ref. 4) suggest that in pure B_2O_3 the boron atoms are triangularly coordinated by oxygens. The basic structural unit consists of a boroxyl ring (B_3O_6), where borons and oxygens alternate on a six-membered ring and the additional three oxygens are dangling off the borons. These units can further network by sharing the dangling oxygens between one another, to form a three-dimensional random network. The existence of the boroxol structure in B_2O_3 glass has been an item of debate for some time. However, the most prominent feature in the Raman spectrum, the intense narrow band at 808 cm^{-1}, could unequivocally be assigned to the planar breathing mode of these rings.[5] The amount of such boroxol rings depends on the temperature and the chemical composition. With the addition of alkali oxides, a fraction of the borons shifts from threefold to fourfold coordination by oxygen, which allows for an increased degree of cross linking within the structure.[6]

Pure B_2O_3 is a relatively "strong" glass former in terms of the strong-fragile classification introduced by Angell.[7] However, its viscosity exhibits a significant deviation from Arrhenius behavior when approaching the glass transition temperature T_g. The viscosity of molten boron oxide has been determined by several investigators, using rotating cylinder viscometry;[8-10] their results are in good agreement with each other. These data show that above 800 °C the viscosity follows an Arrhenius behavior with reasonable accuracy, but that below this temperature the curvature in the $\ln\eta$ vs $1/T$ plot intensifies very noticeably.

The origin of such a non-Arrhenius behavior has been the object of considerable interest. The empirical Vogel-Fulcher relationship, according to which the viscosity varies with temperature as $\exp(DT_0/T-T_0)$, provides for many systems excellent fits to the experimental data. It involves the assumption of another critical temperature, T_0, typically much lower than T_g. Perhaps the most successful model for the explanation of the Vogel-Fulcher relationship is that based on the configurational entropy of the glass.[11] Accordingly, T_0 corresponds to the Kauzmann temperature, at which the entropy of the supercooled liquid equals that of the crystal. This formalism, however, does not incorporate any details concerning the kinetic processes allowing for structural relaxation, or the nature of their gradual arrest when approaching the glass transition.

It is the general perception that above T_g depolymerization of the network occurs. The breakdown of the structural integrity is reflected in the rapidly decreasing rigidity and the increase of mobility. The chief task for understanding glass formation is to link the structural developments that occur above T_g to the mobility of the various structural components present. To date there have been only a few investigations characterizing structures above T_g, i.e., in the supercooled melt region or even at melt temperatures. Recently, Hassan *et al.* were

able to determine for B_2O_3 the fraction of boron atoms incorporated into boroxol rings, based on a careful analysis of Raman spectra.[12] They found this fraction to vary from 0.6 at T_g to 0.25 at 1273 K.

The curvature in the $\ln\eta$ vs $1/T$ plot suggests that different activation energies dominate at different temperature ranges, and hence, that a spread of mechanisms are involved in structural relaxations. The structural changes which occur upon increasing the temperature obviously facilitate the motion of an increasingly larger fraction of the structure. By probing a substance at various frequencies, it is possible to control the spatial extent of the structural feature that is actuated. Relaxational spectroscopy is therefore a promising tool for investigating structural developments in glass-forming systems. Direct mechanical actuation can be realized up to several tens of MHz. For higher frequencies, coupling between probe and the specimen can be established by means of the polarizability of the structural constituents.

Using acoustic loss spectroscopy Kurkjian *et al.* evidenced the strong influence of the OH content on the internal friction in B_2O_3 glass.[13] These authors identified two acoustic loss maxima, one near 50 K and one near 300 K. The peak observed at the higher temperature, reflecting a dissipation mechanism with higher activation energy, is clearly correlated with the presence of water in the glass. Tauke *et al.* performed ultrasonic shear and longitudinal measurements on boron oxide melts at variable frequencies.[14] The ultrasonic velocities and attenuation coefficients were interpreted in terms of a complex mechanical modulus, which allows one to deduct characteristic relaxation times, τ, for the dissipative processes. The data could be fit with a spectrum of relaxation times which follows a normal distribution in $\ln\tau$. These authors were able to attribute the non-Arrhenius behavior in the viscosity to a distribution of relaxation times, which gradually broadens upon decreasing temperature.

Beyond the ultrasonic frequency range, which extends to about 10^7 Hz, mechanical actuation can be realized by means of inelastic scattering of radiation. Brillouin light scattering covers the range between 10^9 and 10^{11} Hz, at wave vectors of around 10^{-2} nm^{-1}. In this experiment light is used as a gauge capable of evidencing oscillating deformations of a structure. Spectral analysis permits the identification of both elastic and dissipative processes. For a given scattering geometry, light scattering operates virtually at constant frequency. With temperature scans, however, one can distinguish between relaxational mechanisms requiring various amounts of thermal activation. In previous high-temperature investigations of boron oxide using Brillouin scattering, the authors have focused in their analysis on the elastic properties of the liquid, or on scattering intensity anomalies. In the present study, we extract both the real and imaginary parts of the complex mechanical modulus from a Brillouin experiment. We show that their magnitudes agree well with those obtained by other methods, provided the appropriate conversions are made. Furthermore, the temperature dependence of the complex modulus, in particular the gradual shift of the energy consumption from elastic to dissipative, reveals information with regard to the structural changes that occur in boron oxide, at and above the glass transition.

II. THEORETICAL BACKGROUND

The scattering of light by condensed matter results from the changes in the dielectric constant associated with density fluctuations. Local changes in density can result from temperature or pressure fluctuations. While the fluctuations due to temperature remain localized, those due to pressure can propagate with the velocity of sound v. Inelastically scattered light appears in the Brillouin spectrum as a doublet of small peaks, which are shifted with respect to the frequency of the incident light by an amount $\pm qv$. The wave vector q of the acoustic phonons probed by the light depends on the scattering geometry according to

$$q = \frac{2n}{\lambda}\sin\theta/2 \ , \tag{1}$$

where n is the refractive index of the liquid, λ is the wavelength of the light, and θ is the angle between incident and scattered light. The frequency shift is a measure of the amount of energy exchanged between photon and phonon; it is positive when the respective wave vectors form an angle larger than 90° and negative otherwise.

As time progresses, the density fluctuations dissipate. Those caused by temperature changes vanish because of thermal diffusion processes, and the propagating pressure waves attenuate because of friction. In either case, the processes involve an energy dispersion, which is reflected in a broadening of the corresponding peaks in the Brillouin spectrum. The width of the Brillouin lines is therefore a measure for the viscous dissipation that occurs on a molecular scale. Quantitative information can be extracted from Brillouin spectra depending on the formalism that is used to relate the spectral line shapes to phenomenological coefficients.

The shape of these lines is described by a dynamic structure factor, $S(\mathbf{q},\omega)$, multiplied by a population probability function. For fluids, the dynamic structure factor can be derived using either the generalized hydrodynamic (GH) formalism[15–17] or the mode coupling theory (MCT).[18–21] MCT gains increasing popularity for the analysis of relaxational phenomena in glass-forming liquids. As opposed to the GH formalism, MCT takes the molecular structure of the liquid into account, in the form of two- and three-body correlation functions. MCT therefore has the potential to furnish more accurate results, however, it also has the inconvenience of requiring more detailed information about the structure of the system under consideration. Regardless of the assumptions made in either GH or MCT, the structure of the expression for the dynamic structure factor is quite similar in both cases. In the expression for $S(\mathbf{q},\omega)$ derived from MCT, the phenomenological transport coefficients are expressed explicitly as time correlation functions, while in GH a simple exponential decay is assumed for the time dependence of these coefficients.

We will base the present analysis on the expression derived from the GH formalism because in terms of the in-

formation contained in our data, no advantage would result from using the somewhat more complicated MCT expressions. In the GH approach, the expression for $S(\mathbf{q},\omega)$ can be obtained by simultaneously solving the equation of continuity, the linearized Navier-Stokes equation, and Fourier's second law, which describe in this sequence the mass, momentum, and energy balances. As an important additional assumption in this approach, the viscosity coefficient, η, which appears in the momentum balance, is assumed to depend on time as $\eta(t)=\eta_0 e^{-t/\tau}$. After extensive manipulations, the normalized scattering intensity is found to be

$$\frac{S(\mathbf{q},\omega)}{S(\mathbf{q})}=\frac{2(\gamma-1)}{\gamma}\cdot\frac{q^2\cdot\kappa/\rho_0 c_p}{\omega^2+(q^2\cdot\kappa/\rho_0 c_p)^2}+\frac{1}{\gamma}\left[\frac{q^2\cdot\Gamma}{(\omega+vq)^2+(q^2\Gamma)^2}+\frac{q^2\cdot\Gamma}{(\omega-vq)^2+(q^2\Gamma)^2}\right], \tag{2}$$

where $\gamma=c_p/c_v$,

$$\Gamma=\frac{1}{2}\left[\frac{\eta'(\omega)}{\rho_0}+\left[\frac{\kappa}{\rho_0 c_0}\right]\right]\cdot(\gamma-1),$$

ρ_0 is the average density, κ is the thermal conductivity, c_v is the heat capacity at constant volume, and c_p that at constant pressure. The coefficient $\eta'(\omega)$ is the dynamic viscosity, and corresponds to the real part of the Fourier transform of the time-dependent viscosity, $\eta(t)$. The ratio $(\kappa/\rho_0 c_p)$ is the thermal diffusivity, but it may be perceived in the broader sense as describing the diffuse behavior of density or concentration, including the transport of matter. The first term on the right-hand side of Eq. (1) corresponds to the Rayleigh peak and the next two terms represent the anti-Stokes and Stokes lines of the Brillouin components.

In the context of the present study, our principal interest lies in the structural developments within the supercooled liquid. Changes of the chemical bonding within the structure will affect its rigidity (or elasticity), as well as the mobility of structural components which contribute to viscous dissipation. A measure which combines both elasticity and dissipation is given by the complex mechanical modulus[22]

$$M^*(\omega)=M'+iM''=M_0+M_2\frac{\omega^2\tau^2}{1+\omega^2\tau^2}+iM_2\frac{\omega\tau}{1+\omega^2\tau^2}. \tag{3}$$

Here, M_0 is the static modulus and M_2 is the relaxational modulus. If M_∞ is the modulus at infinite frequency, and M_0 that at zero frequency, then the magnitude of the relaxation modulus is given by $M_2=M_\infty-M_0$. For a longitudinal actuation, each component of the modulus includes a bulk and a shear modulus, $M=K+4/3G$. For liquids, the Brillouin spectrum provides access to both components of the complex modulus. The real part of the modulus, which represents the capability of the structure to store energy elastically, can be related to the frequency shift experienced by the inelastically scattered light. Denoting by ω the frequency difference between Rayleigh and Brillouin lines, $\omega=|\omega_B-\omega_R|$, we get

$$\frac{\rho_0\omega^2}{q^2}=M_0+M_2\frac{\omega^2\tau^2}{1+\omega^2\tau^2}. \tag{4}$$

The imaginary part of the complex modulus is a measure of the energy dissipated by friction. It is related to the dynamic viscosity, $\eta'(\omega)$, according to

$$\eta'(\omega)=M_2\frac{\tau}{1+\omega^2\tau^2}. \tag{5}$$

According to Eq. (2), the width of the Brillouin peak is predominantly controlled by this viscosity. The full width at half height of the Rayleigh peak is

$$\Delta\omega_R=2\frac{q^2\cdot\kappa}{\rho_0 c_p}, \tag{6}$$

while that of the Brillouin peak is

$$\Delta\omega_B=2q^2\cdot\Gamma=q^2\cdot\left[\frac{\eta'(\omega)}{\rho_0}+\left[\frac{\kappa}{\rho_0 c_p}\right]\cdot(\gamma-1)\right]. \tag{7}$$

By combining both expressions, and by using the relative intensities of Rayleigh and Brillouin peaks (Landau-Placzek ratio) to estimate the value of γ, the viscosity is obtained as

$$\nu'(\omega)=\frac{\eta'(\omega)}{\rho_0}=\frac{1}{q^2}\cdot\left[\Delta\omega_B-\frac{\Delta\omega_R}{2}\cdot\frac{I_R}{2I_B}\right]. \tag{8}$$

For a constant scattering geometry, the Brillouin probe essentially operates at constant frequency. The technique is therefore poorly suited to provide the full frequency dependence of M^*. On the other hand, a variation of temperature will produce a similar effect. In Eqs. (3)–(5), τ is the characteristic time constant for the relaxational process. For thermally activated processes, τ can be expressed as an Arrhenius function,

$$\tau=\tau_0 e^{E_A/k_B T}. \tag{9}$$

Substitution into Eq. (3) yields

$$M^*(\omega,T)=M_0(T)+M_2\frac{\omega^2\tau_0^2 e^{2E_A/k_B T}}{1+\omega^2\tau_0^2 e^{2E_A/k_B T}}+iM_2\frac{\omega\tau_0 e^{E_A/k_B T}}{1+\omega^2\tau_0^2 e^{2E_A/k_B T}}. \tag{10}$$

Finally, if processes of a different nature occur simultaneously, the system's response can be characterized by a distribution of relaxation times, $g(\tau)$, and the above expression becomes

$$M^*(\omega,T)=M_0(T)+M_2\int_0^\infty g(\tau)\frac{\omega^2\tau_0^2 e^{2E_A/k_BT}}{1+\omega^2\tau_0^2 e^{2E_A/k_BT}}d\tau$$

$$+iM_2\int_0^\infty g(\tau)\frac{\omega\tau_0 e^{E_A/k_BT}}{1+\omega^2\tau_0^2 e^{2E_A/k_BT}}d\tau\ . \qquad (11)$$

Note that the spectrum for shear relaxations is not necessarily the same as that for volume relaxations. Consequently, one would need to formally expand the relaxational modulus into its shear and bulk components, and weigh each component with the proper distribution function. Oftentimes, the difference in relaxation time spectra is negligible, especially when the shear modulus outweighs the bulk modulus. In the analysis below, we make use of this simplification. In Fig. 1, we show the temperature and frequency dependence of the complex mechanical modulus. Figure 1(a) is a plot of the real component, and Fig. 1(b) is a plot of the imaginary component of this modulus. Using a logarithmic scale for the frequency axis makes the two variables almost interchangeable. Figure 1(a) shows that at high frequencies and low temperatures the rigidity of the structure is large, whereas at low frequencies and high temperatures the system appears fluid. The transition between a rigid and fluid behavior is characterized by an inflection point in the real part and a maximum in the imaginary part of the complex modulus. The temperature at which the imaginary part of the modulus reaches this maximum depends on the probing frequency according to

$$T_m=\frac{-E_A}{k_b\ln(\omega\tau_0)}\ . \qquad (12)$$

There is an important difference between the two variables ω and T: When increasing the frequency while keeping the temperature constant, the structure is subject to mechanical actuation only. Given sufficient time for the structure to relax during each period of the imposed constraint, i.e., $\omega\cdot\tau<1$, the system is displaced from thermal equilibrium by the amount of energy introduced by the probe. In the other extreme, when $\omega\cdot\tau>1$, the time of each period is too short for any displacement to take place. Instead of dissipating the energy for molecular transport, it is elastically stored in a structure whose geometry remains close to that assumed in thermal equilibrium. On the other hand, when increasing the temperature, while probing the system at constant frequency, the structure is modified due to a shift in the thermal equilibrium. At low temperature strong chemical bonds prevail and the structure cannot undergo relaxation. At high temperature, these bonds are weakened by means of thermal energy. Certain structural components become mobile, and the system complies to the imposed constraint. In this case the change in the dynamical response of the system depends on the change in equilibrium structure, while in the previous case the thermal equilibrium is unaltered, and the compliance of the structure depends on the rate with which a constraint is applied. Hence, if the equilibrium structures at high and low temperatures are characterized by a significantly different geometry the applicability of Eq. (10) to describe the thermal relaxation of the system is not warranted, since essentially a different substance is probed when the system exhibits compliant as opposed to rigid behavior. This is certainly the case if phase transformations occur within the temperature interval. On the other hand, this possible limitation offers an interesting opportunity for the exploration of phenomena such as the glass transition.

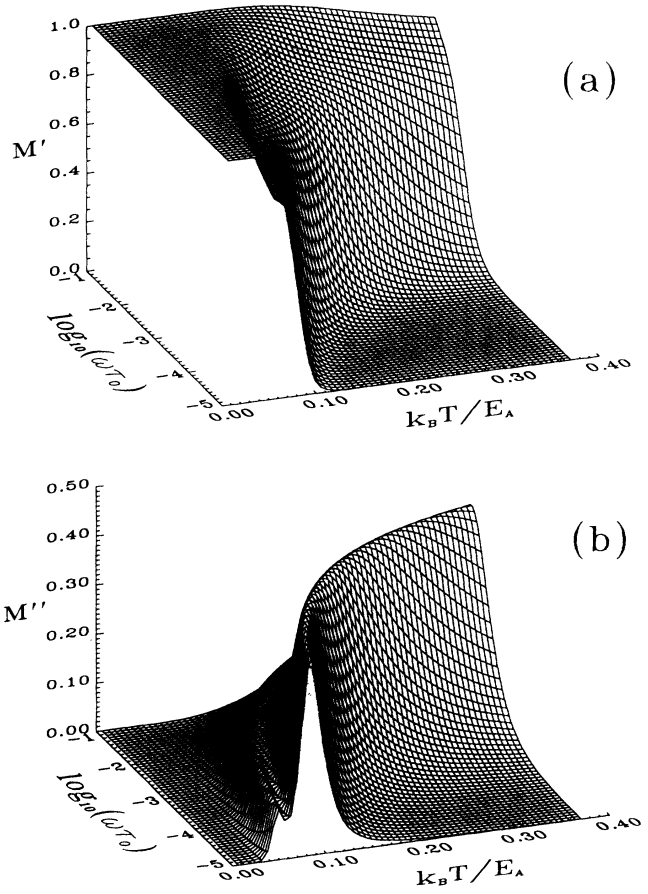

FIG. 1. (a) Schematic of the real component of the complex mechanical modulus, as a function of the normalized temperature, k_BT/E_A, where E_A is the activation energy of the relaxation process, and the normalized frequency, $\omega\tau_0$, where τ_0 is the time constant of the process. Two hypothetical mechanisms are superimposed. (b) Schematic of the imaginary component of the complex mechanical modulus, as a function of the normalized temperature, k_BT/E_A, where E_A is the activation energy of the relaxation process, and the normalized frequency, $\omega\tau_0$, where τ_0 is the time constant of the process. Two hypothetical mechanisms are superimposed.

III. EXPERIMENTAL PROCEDURE

The borate glasses were prepared from powders of boric acid and alkali carbonates, with a total impurity content of less than 0.2% by weight. The powders were suspended in water-free ethanol, and intimately mixed. The mixture was then heated and, immediately after evaporation of the ethanol, melted in a platinum crucible. After about 1 h of homogenization in air, the melts were quenched and crushed. The glasses were then remelted

and the Brillouin sample holders were filled with material simply by immersing these into the molten glasses. The sample holders consist of platinum-rhodium wire bent in the form of a double-loop spiral. This form allows for an optimal containment of the liquid with a minimum of surrounding material, and resulted in a minimal scattering from the platinum surface. Suspended by surface forces, the liquid assumes the shape of a slightly bulged cylinder of about 2.5 mm height and 3 mm diameter. The menisci that form at the surfaces through which passed the incident and scattered light, were sufficiently flat to conserve the 90° scattering geometry. The light beam entered through the bottom and the scattered light was collected laterally, at about half height of the cylindrical droplet.

For the high-temperature measurements, samples were suspended in a small furnace which was heated by a platinum coil. The furnace has a cylindrical bore in the bottom and top parts of the insulation material. The incident light enters through the lower bore, and the upper bore is necessary to permit the unscattered light to leave the sample chamber. The scattered light, on the other hand, exits the furnace horizontally through a conical orifice in the side wall. A collimating lens collects the scattered light over a 15° solid angle, with an average scattering angle of 90°. The orifices in the stainless-steel housing, on the bottom, side, and top of the furnace are sealed by means of fused silica windows, in order to allow for a controlled gas atmosphere during the experiments.

Prior to collecting spectra, the samples were heated to the highest temperature, i.e., 1150–1200 °C, and held there for about 8 to 12 h. The sample chamber was purged with dried air, containing less than 3 ppm of water. This equilibrium period was necessary to reduce the water content in the melts to a minimum. Borates are highly hygroscopic, and one risks adsorbing water on the specimen's surface during the handling between sample preparation and measurement furnaces. The chemical composition of the samples was determined after the Brillouin measurement by gas chromatography. Comparison with the original batch composition typically showed an agreement within 1 mol %.

Subsequently the samples were cooled and held at temperature intervals of about 20 °C. Spectra were collected after thermal equilibration was reached. The collection of a typical spectrum took between 3 and 5 min. None of the samples crystallized during these cooling schedules, which would have been immediately obvious through dramatic changes in the scattering intensities and frequency shifts. For comparison sake, select measurements were repeated upon reheating the samples. Within the range of the experimental accuracy, no significant hysteresis was detected. The slow cooling rates that these samples were subject to resulted in relatively relaxed glass specimens. One might expect stronger differences between cooling and heating cycles in case the samples were quenched more rapidly. Currently, our sample chamber does not allow for very rapid cooling, so that the effect of varying fictive temperatures of the glass on its mechanical and relaxational behavior could not be studied.

The incident light was produced by a single-mode Argon laser at a wavelength of 0.5145 μm. The linewidth of the incident light is approximately 250 MHz. The scattered light was analyzed using a six-pass tandem Fabry-Perot interferometer.[23] The quality of mirrors used in the current setup produces a reflectivity finesse of about 150. The intensity of the filtered light was measured with a Thorne EMI photomultiplier tube, and recorded on a 1024-channel multichannel analyzer.

The raw spectra were then deconvoluted to eliminate the broadening that results from the imperfections in the optical components and the interferometer. The deconvolution was accomplished in reverse manner, i.e., by fitting the result of a convolution of Lorentzians with a Gaussian broadening function to the data. In this process the parameters to be optimized were the total peak intensity, its location on the frequency scale, and the full width at half height (FWHH). The instrumental broadening, expressed as the variance of the Gaussian, was determined from the Rayleigh line of a blank experiment, where the sample was replaced by a mirror.

IV. RESULTS

In the following we report our measurements of the longitudinal elastic moduli and the dynamic viscosities of pure boron oxide and several binary alkali borate systems. Our analysis evolves around the pure boron oxide. This system has been extensively investigated by other techniques, providing the necessary information for the interpretation of our results. The data for select binary alkali borate systems were also analyzed, to further substantiate the interpretation of our results.

In Fig. 2, the Brillouin spectra of a sodium borate sample, containing 14 mol% of sodium oxide, are shown for various temperatures. Only the anti-Stokes tails of the

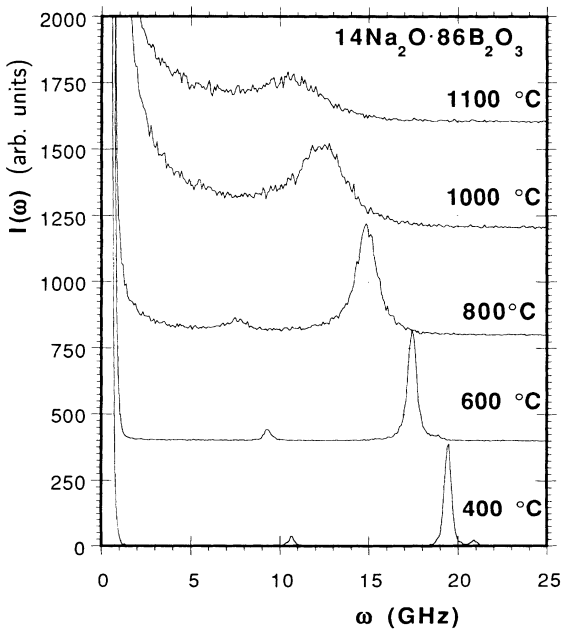

FIG. 2. Anti-Stokes branches of the Brillouin spectra for a sodium borate system, containing 14 mol % Na_2O, at various temperatures.

spectra are displayed, and their baselines are offset for better visibility. Two features become immediately apparent: (i) the frequency shifts of the Brillouin lines decrease, and (ii) the widths of these peaks increase with increasing temperature. The latter trend reveals a decrease of the real and an increase of the imaginary component of the complex modulus with increasing temperature. The longitudinal elastic moduli are obtained by evaluating the left-hand side of Eq. (4). The frequency shift is taken from the Brillouin spectra, while the density and the refractive index, which is required to calculate the magnitude of the scattering vector, according to Eq. (1), are taken from the literature.[24] In the case of pure boron oxide, both parameters are available as a function of temperature. For almost all binary compositions, we could find density values as a function of temperature. For those compositions where this information was not available, we took values for the bracketing compositions and interpolated linearly. The same procedure was followed for the room temperature refractive indices. Since the temperature dependence of the refractive indices for binary borates was unavailable, we used that for pure B_2O_3 as a first approximation. We do not expect any significant error from this substitution, since the total change in the refractive index, over the entire temperature range, for B_2O_3 as well as for some multicomponent glasses, is less than a percent.

The longitudinal elastic moduli for various systems are shown in Fig. 3. These values correspond to the sum of the static modulus and the real part of the dynamic modulus. The room temperature values of this modulus increase with increasing alkali concentration. For each composition, the modulus remains nearly constant until T_g is reached. T_g is characterized by a discontinuity in the temperature dependence of the elastic modulus. Above T_g the modulus drops with increasing temperature. The rate of decrease grows with increasing alkali concentration. The high-temperature values of the elastic modulus for the various compositions appear to converge at a value of approximately 10 GPa. Note that the modulus for pure B_2O_3 levels off between 900 and 1100 °C, but above that temperature it begins to decrease again. The curves for the moduli of the binary borates decrease steadily, but exhibit changes in curvature.

The kinematic viscosities are evaluated from the Brillouin and Rayleigh peak widths according to Eq. (8). These viscosities describe the friction attributable to structural elements that move within the time frame defined by the probing frequency. Multiplied with the probing frequencies, these viscosities yield the amount of energy dissipated per unit mass. We will refer to these quantities as specific loss moduli. Their values are shown in Fig. 4. The initial trend above T_g reflects an increase of dissipation with increasing temperature. For specimens with high alkali concentration, the data exhibit a maximum, as one would expect based on Fig. 1(b). The temperature at which this maximum occurs, given by Eq. (12), depends linearly on the activation energy of the process that causes dissipation.

In Fig. 5, the specific loss moduli of pure B_2O_3 samples equilibrated with different gas atmospheres are shown. In addition to dry air, containing about 3 ppm of moisture, B_2O_3 samples were brought into equilibrium with air that contained about 2% by volume water vapor (i.e.,

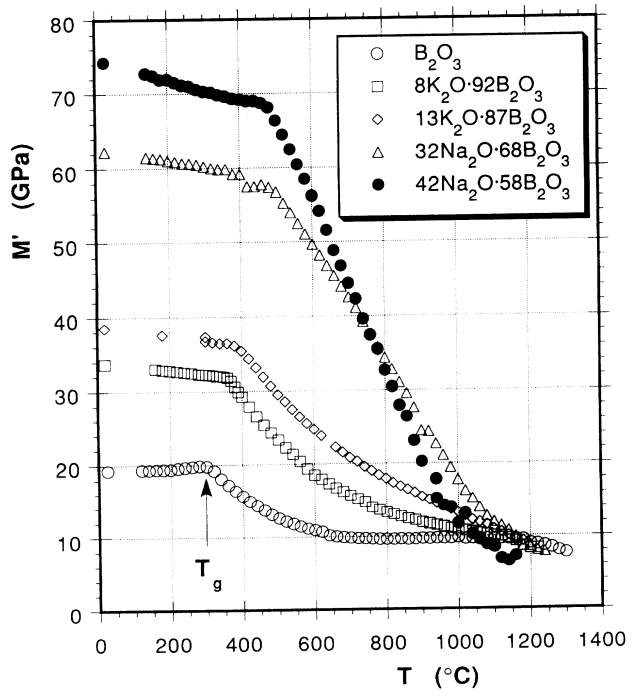

FIG. 3. Longitudinal elastic modulus for B_2O_3 and for various binary alkali borates, as a function of the temperature. The discontinuity in the temperature dependence of this modulus reflects the glass transition temperature.

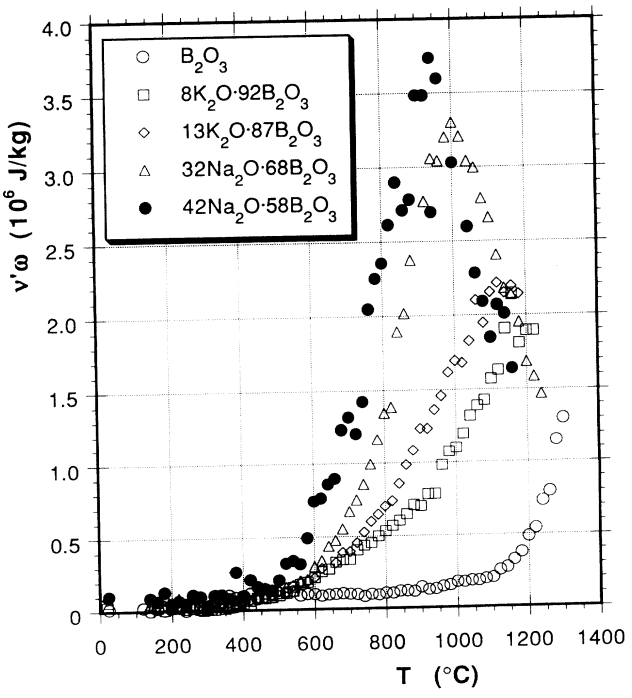

FIG. 4. Specific loss modulus for B_2O_3 and for various binary alkali borates, as a function of the temperature.

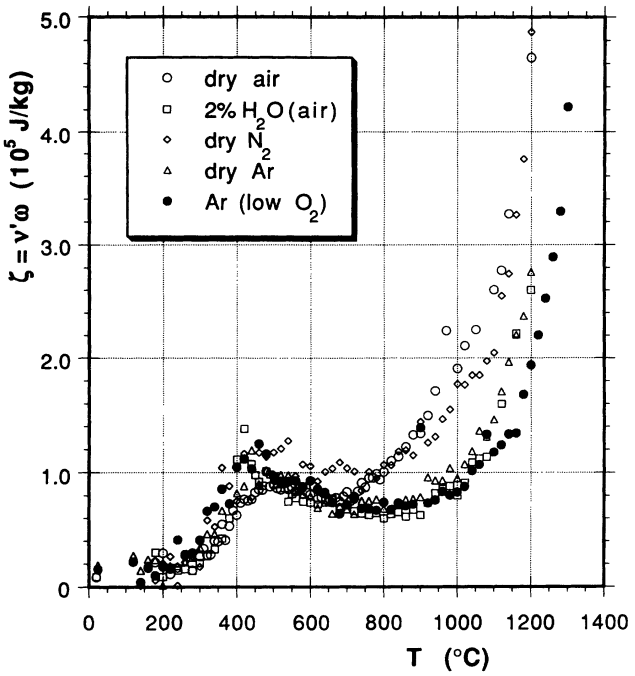

FIG. 5. Specific loss modulus for B_2O_3, equilibrated with various gas atmospheres (○, dry air; ◇, dry nitrogen; △, dry argon; ●, dry argon with reduced oxygen partial pressure, and □, air containing 2% water vapor), as a function of the temperature.

saturated at room temperature), pure nitrogen and pure argon. The water content of the argon and nitrogen was also approximately 3 ppm, while their oxygen partial pressure was 5×10^{-6}, according to specification. In a separate experiment, the argon was passed through copper shavings heated to 400 °C, which reduced the oxygen partial pressure to an estimated 10^{-9}.[25] In the data for all B_2O_3, a small hump is clearly visible at about 500 °C, which indicates that several mechanisms contribute towards dissipation, and their maximum activation occurs at different temperatures. While the temperature and the magnitude of the small hump remain virtually unaffected by the gas composition, the increase of the specific loss modulus towards higher temperatures occurs more or less rapidly, depending on whether nitrogen is present in the atmosphere or not.

V. DISCUSSION

Multiplication of the specific loss moduli with the specimen densities yield the imaginary components of the mechanical moduli. The loss moduli for pure B_2O_3 and for two potassium borate specimens, calculated from the data presented in Fig. 4, are shown in Fig. 6(a). The corresponding real components of the complex modulus are plotted in Fig. 6(b), along with theoretical curves calculated based on the fitting procedure described in the following. According to the model described in Sec. II, one would expect the data shown in Figs. 6(a) and 6(b) to follow a temperature dependence described by Eq. (11). Since the distribution of relaxation times, $g(\tau)$, is not known, we proceeded to fit the data with a linear combination of individual terms, i.e.,

$$M^*(\omega,T)=M_0(T)+M_2\sum_m g_m\frac{\omega^2\tau_{0,m}^2 e^{2E_{A,m}/k_bT}}{1+\omega^2\tau_{0,m}^2 e^{2E_{A,m}/k_BT}}$$

$$+iM_2\sum_m g_m\frac{\omega\tau_{0,m}e^{E_{A,m}/k_BT}}{1+\omega^2\tau_{0,m}^2 e^{2E_{A,m}/k_BT}}\,. \qquad (13)$$

In this procedure, for which we used a Marquard-Levenberg algorithm, we optimized the preexponential time constants $\tau_{0,m}$, the activation energies $E_{A,m}$, and the weighing factors g_m. Because the preexponential and exponential factors in Eq. (13) have a different influence on the magnitude of M^*, the optimization of these parameters represents a numerical challenge. Fairly close initial guesses are required. For this reason, we limited our analysis to the minimum number of basis functions necessary to provide a reasonable fit to the data. Typically, the use of three to five basis functions gave satisfactory results. When more basis functions are used, the outcome of the fitting procedure strongly depends on the initial guesses, and the resulting set of optimized parameters tends to no longer be unique. Even though curves can be generated that fit the data more closely, the use of more basis functions does not improve the insight that can be gained. The fitting procedure is illustrated in Fig. 6. In each case three terms were used in Eq. (13). The solid lines in Fig. 6(a) represent the loss moduli associated with individual relaxation mechanisms, and the dotted lines correspond to the sum of the solid lines for each sample. Similarly, in Fig. 6(b) the dotted lines represent the total rigidity of a given system, resulting from a linear combination of individual terms. The solid lines, representing individual relaxation mechanisms, are superimposed onto the data such that their baselines correspond to the effective static modulus, valid at that temperature.

We will first discuss the loss moduli. The activation energies and the preexponential time constants are listed in Table I, along with those found for the binary compositions. In pure B_2O_3, the small dissipation maximum at about 500 °C is characterized by an activation energy of 36.5 kJ/mol. A second hump, which is of small intensity and peaks at about 750 °C, has an activation energy of 44.8 kJ/mol. The highest activation energy, 67.3 kJ/mol, describes the continuous increase in viscous dissipation towards the upper end of the temperature scale. For systems with low alkali contents, a maximum is not reached within the temperature range covered by our experiments, or even within the stability range of these liquid phases. However, by fixing the onset and the slope of the ascending flank of an activation peak, the available data allow for a fairly unequivocal determination of the corresponding parameters. The aforementioned activation energies are fairly distinct. This leads us to the conclusion that they describe independent mechanisms, which gradually become activated as the temperature is raised.

The challenge consists in developing a description of the molecular scale processes involved in these dissipa-

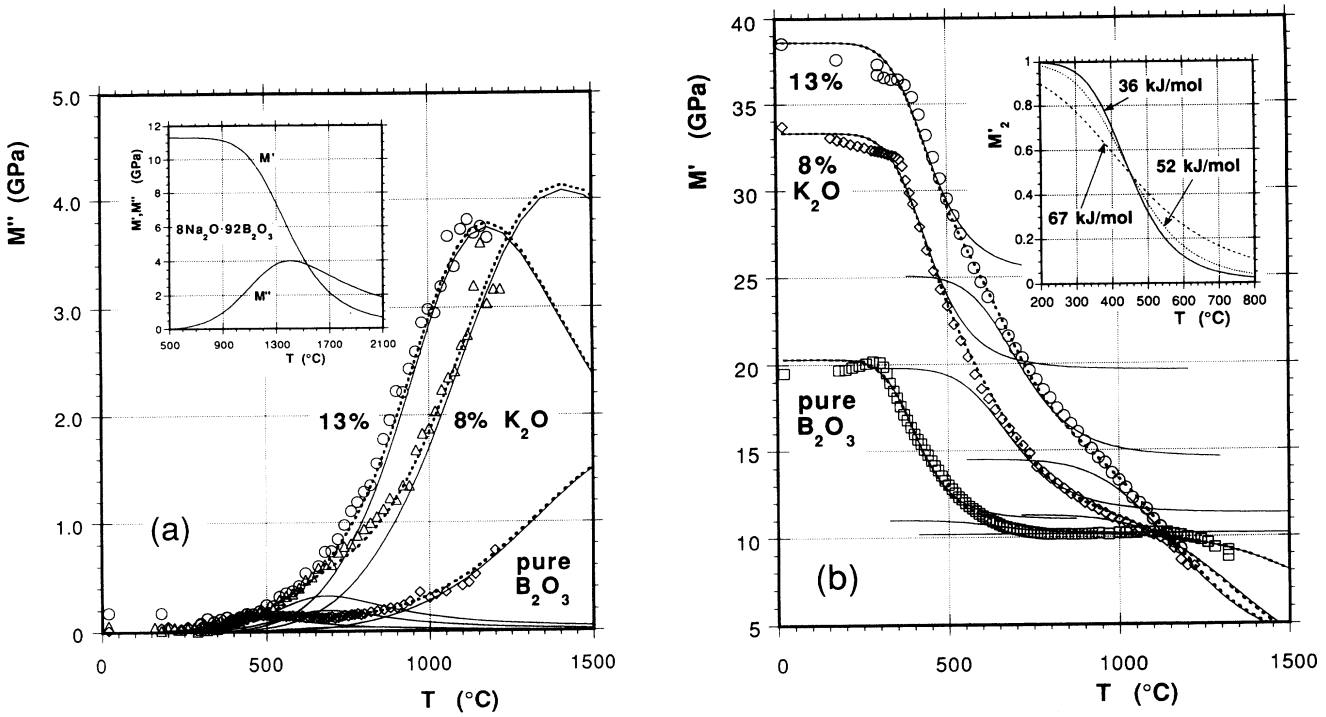

FIG. 6. (a) Illustration of the fitting procedure for the imaginary component of the complex mechanical modulus for B_2O_3 and for two binary potassium borates. Symbols represent the experimental data, thin solid lines represent individual dissipation mechanisms, and the dashed line results from the linear combination of the curves for individual mechanisms. Inset: Comparison between real (M') and imaginary (M'') components of the complex mechanical modulus for the high-activation energy mechanism in a binary potassium borate. (b) Illustration of the fitting procedure for the real component of the complex mechanical modulus for B_2O_3 and for two binary potassium borates. Symbols represent the experimental data. The thin solid lines, which represent individual dissipation mechanisms, are superimposed on the experimental data with a base level corresponding to their respective static modulus. The dashed line results from the linear combination of the curves for individual mechanisms. Inset: Comparison between the transition between low- and high-temperature moduli controlled by different activation energies. The curves are shifted so that the inflection points coincide.

tion mechanisms. The light scattering probe selects high-frequency phonons; viscous dissipation is due to aperiodic occurrences within these vibrations, and can only be observed if significant relaxation takes place during each period of these vibrations. This means that the perturbance has to have small spatial extents, i.e., of the order of molecular displacements that can be completed within a nanosecond. Dissipation mechanisms that can be observed with this technique therefore include diffusive atomic displacements and aperiodic vibrations of small and weakly bonded structural segments. The corresponding viscosity coefficients measure the amount of momentum transported by these entities. For the assignment of a dissipation maximum to a particular mechanism, it is in general necessary to introduce information from complementary experiments, or from computer simulations. We employed this strategy successfully in previous investigations,[26] where we were able to identify the alkali cation diffusion in alkali silicate melts, through comparison with torsional pendulum internal friction data.

TABLE I. Activation energies and preexponential time constants for the three principal relaxation mechanisms in B_2O_3 and binary alkali borates.

Composition	$\omega\tau_0$	E_A (kJ/mol)
Pure B_2O_3	2×10^{-2}	67.3
	3×10^{-3}	44.8
	3×10^{-3}	36.5
1% K_2O	2×10^{-2}	67.3
	3×10^{-3}	44.0
	3×10^{-3}	36.5
8% K_2O	8×10^{-3}	67.3
	3×10^{-3}	46.6
	3×10^{-3}	36.0
13% K_2O	4×10^{-3}	67.3
	3×10^{-3}	49.8
	3×10^{-3}	36.0

The determination of the activation energies and preexponential time constants, by fitting Eq. (13) to the Brillouin data, allows one to compare the high-frequency dynamic viscosity with that determined by other methods, after substituting Eq. (8) in Eq. (5) and after using different values for the frequency. This comparison is made in Fig. 7. In Fig. 7(a), the breakdown of the specific loss modulus for B_2O_3 into the contributions from individual relaxation mechanisms, as determined from Brillouin linewidths, is shown. Each curve is then converted

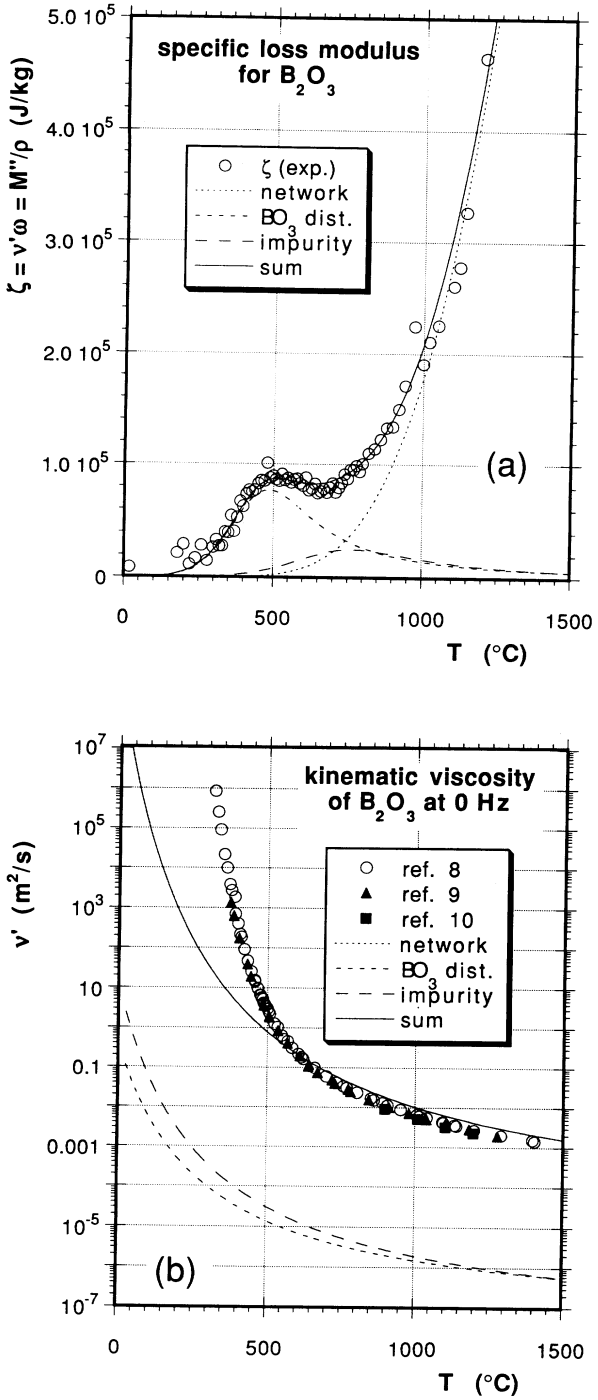

FIG. 7. (a) Specific loss modulus for B_2O_3, as a function of the temperature, and illustration of the fitting procedure. Dashed lines represent the individual mechanisms, which are attributed to (i) final network disintegration, (ii) nonplanar BO_3 distortions, and (iii) impurity diffusion. The solid line results from the linear combination of the curves for individual mechanisms. (b) Kinematic viscosity for B_2O_3, as a function of the temperature, resulting from the data shown in (a), after conversion to zero frequency. Comparison is made with data from rotating cylinder viscometry from Refs. 8–10 (symbols). Dashed lines represent the individual mechanisms, which are attributed to (i) final network disintegration, (ii) nonplanar BO_3 distortions, and (iii) impurity diffusion. The solid line results from the linear combination of the curves for individual mechanisms.

into a kinematic viscosity at zero frequency. The results are plotted in Fig. 7(b) as dashed lines, where they are compared to the viscosity data determined by rotating cylinder viscometry (symbols), as reported by three independent investigators.[8–10]

The solid line in Fig. 7(b) results from the linear combination of the viscosities that can be attributed to the different relaxation mechanisms, using the same weighing factors that were obtained when fitting the data in Fig. 7(a). The two lower activation energy mechanisms contribute very little to the total viscosity. These individual viscosities are 4 orders of magnitude smaller than the one corresponding to the high activation energy mechanism. The latter is actually indistinguishable from the total viscosity, within the resolution of this graph. Above 500 °C the agreement between the viscosities determined by rotating cylinder viscometry and those derived from the line shape of a Brillouin spectrum is fairly good. Actually, complete agreement is not to be expected, since the Brillouin data furnishes a viscosity that comprises bulk and shear viscosity, i.e., $\eta'(\omega)=\eta'_B(\omega)+4/3\eta'_S$, whereas the rotating cylinder method only yields the shear viscosity. Typically, the bulk viscosity is small in comparison to the shear viscosity, however, it can definitely account for the observed difference between the viscosity from the Brillouin experiment and those from rotating cylinder viscometry.

Below 600 °C, the viscosity determined from Brillouin spectra deviates from the rotating cylinder viscometry data. At the same time, 600 °C marks the onset of the high-activation energy dissipation mechanism [see Fig. 7(a)], which is predominantly responsible for the zero-frequency viscosity derived from the high-frequency measurement [solid line in Fig. 7(b)]. Above 600 °C, the processes that cause viscous dissipation come to a completion within less than a nanosecond, so that the viscosities appear to be the same, whether the substance is probed at 0 Hz or at 10 GHz. Below that temperature, on the other hand, additional energy is dissipated by processes which have significantly longer relaxation times than the Brillouin probe is able to cover. Between 300 and 500 °C the light scattering experiment and the rotating cylinder technique clearly probe different processes. Brillouin scattering monitors the thermal decomposition of the network structure. It does not cause the system to deviate noticeably from its thermodynamic equilibrium. On the other hand, a liquid confined between two surfaces that move relative to each other experiences significant shear stresses. The mechanical energy introduced into the specimen causes structural deformation, and nonequilibrium configurations are produced. Part of the resistance measured by the viscometer is due to the rupturing of network bonds.

As is obvious from Fig. 6(a), the dissipative mechanism, which is first activated above the glass transition, is the one with the lowest activation energy. This is not surprising, since the lower the temperature the smaller the amount of thermal energy available for such activation. It is noteworthy that, since the slopes of the curves in Fig. 7(b) are a measure for the magnitude of the activation energy, the rotating cylinder measurements appear

to indicate a larger activation energy for the relaxation processes immediately above T_g, and a smaller activation energy for the high-temperature processes. This finding presents a contradiction, when comparing Figs. 7(a) and 7(b). Above 600 °C the viscous dissipation shown in Fig. 7(a) is dominated by the 67-kJ/mol mechanism. In this temperature range the findings of the high-frequency probe, after conversion, agree with those from the rotating cylinder viscometry. Below 600 °C, on the other hand, the high-frequency dissipation is governed by the 36-kJ/mol mechanism, while the rotating cylinder viscosity appears to have an activation energy of more than 80 kJ/mol. The torque sensed by the rotating cylinder viscometer not only reflects the stress generated due to the relative motion of layers of fluid in thermal equilibrium, but in addition, the stress required to produce structural modifications necessary to maintain the imposed shear rate. Since it causes virtually no perturbance in the structure of the probed sample, the Brillouin scattering measurement furnishes viscosity data close to the zero-shear rate limit. The mechanism which is active under this condition immediately above T_g contributes vanishing amounts to the dissipation when converted to zero frequency, and is unlikely to be resolved with a steady shear rate measurement. The small activation energy characterizing this mechanism points towards the motion of a small structural entity, which, in a room temperature glass is confined to the energetically least favorable site, and is released upon passage through T_g.

With this in mind, let us examine the real component of the complex mechanical modulus, i.e., the capability of the structure to store energy elastically. T_g marks the onset of the transition between low- and high-temperature limits of the elastic modulus. This transition, which involves the depolymerization of the borate network, is most rapid immediately above T_g. The theoretical curve describing this transition, i.e., the real term in Eq. (10), exhibit an inflection at about 1.1 times the temperature where the maximum in dissipation occurs. While the activation energy controls the temperature at which the transition between low- and high-temperature elastic moduli occurs, the preexponential term controls the slope at the inflection point, i.e., the rate with which transition occurs. The lower the τ_0, the lower the inflection temperature, and the more rapid the transition. For high activation energies the inflection temperature shifts upwards, and the range over which the transition occurs broadens. In the inset of Fig. 6(b) the transitions controlled by different combinations of activation energies and preexponential coefficients are compared, after shifting the curves on the temperature axis such that the inflection points coincide. Hence, the steep initial drop in elasticity suggests that the loss of a significant portion of the rigidity of the equilibrium structure unmistakably involves a process characterized by a low activation energy and a low time constant.

The data shown in Fig. 6(b) can again be modeled by a linear combination of relaxation terms given by the first summation in Eq. (13). The use of a single term leads to a much poorer agreement. The important finding of this analysis is that the fits are realized with the same activation energies and time constants than those determined for the dissipation peaks. The static modulus, M_0, is a function of the temperature. For each mechanism it corresponds to the sum of the relaxational moduli of all processes activated at higher temperatures. Furthermore, the same low activation energy that describes the initial decrease in the elastic modulus above T_g for pure B_2O_3 applies for all binary compositions. This agreement imparts justification to the use of the relaxation formalism expressed by Eq. (3), after substitution of an Arrhenius term for the relaxation time, in order to describe the phenomena involved in the glass transition. The agreement is actually surprising, since the transition between the supercooled and the molten state implies significant structural changes upon depolymerization. With this change in bonding topology one would expect to encounter a different substance at high temperatures than at low temperatures, at least from a mechanical point of view. The applicability of a relaxation formalism therefore establishes an interesting correspondence between the departure from equilibrium of a structure due to mechanical deformation, and the change of the equilibrium mechanical properties due to structural changes upon introduction of thermal energy.

The recent Raman scattering study by Hassan *et al.*[12] substantiates the assumption that the network degradation in borates is associated with the opening of boroxol rings. According to these authors' findings, the decrease in the fraction of boron atoms incorporated in boroxol rings is initiated at T_g. The fraction continues to drop gradually until it levels at about 1300 °C. This gradual opening of boroxol rings suggests a spread of structural environments for these entities. The present investigation complements the work by Hassan *et al.* in that it provides insight into the structural developments on an intermediate- and long-range scale. Obviously, the small amount of energy dissipated in the process that we observe in the broadening of the Brillouin line is insufficient to account for the breaking of boron-oxygen bonds. It is important to realize that the light scattering probe is based on the interaction between phonons and photons, during which a minute amount of energy is exchanged. This energy is sufficient to invoke the motion of moieties which are set free (i.e., brought near the saddle point of the activation barrier), at least temporarily, during the thermally activated network breakdown. The displacement of these moieties are part of the fluctuations that establish a dynamic equilibrium. The characteristic time constant of this process corresponds to a resonant frequency of about 110 cm^{-1}, which points towards a vibrational motion involving more than one atom, possibly a rotational or a rocking mode of weakly bonded species.

The real component of the complex modulus indicates that the low-activation energy peak is associated with the rapid network disintegration above T_g, a process which involves the conversion of B-O-B units which belong to boroxol rings, either into B-O-B units that are part of a more open structure, or into singly bonded oxygens (B-O units). The latter possibility implies the formation of a defect that would be facilitated by an excess of oxygen, while the former calls for the simultaneous rup-

ture of two B-O bonds, followed by an immediate recombination after switching neighbors. This mechanism is sterically much more constrained. Excess oxygen could be brought into the systems as molecular oxygen, or as water molecules. We therefore examined the influence of both of these species on the temperature dependence of the mechanical modulus, by varying their partial pressure in the atmosphere with which the samples were equilibrated.

The dissolution of water molecules can have two consequences. On the one hand, it contributes to the breakdown of the network by introducing terminal hydroxyl groups. On the other hand, hydrogen is highly mobile and can serve as a vehicle for momentum transport. Both effects could potentially facilitate a low-energy dissipation mechanism. Kurkjian and Krause, when performing acoustic loss measurements, observed a strong enhancement of a loss mechanism due to the presence of water in B_2O_3.[13] This mechanism, whose activation energy is 26.3 kJ/mol (i.e., lower than what we observed), has also been observed in dielectric loss measurements.[27] These authors did not specify where the loss is due to changes in the network structure, upon introduction of water, or to the motion of a small unbonded dissolution product, such as hydrogen cations. The comparison between "dry" and "wet" boron oxide in our experiment shows that, although the low-energy dissipation is somewhat intensified in the wet specimen, it is the high-energy mechanisms that are significantly more affected (see Fig. 5). Consequently, we rule the momentum transported by diffusing hydrogen out, as the cause of our low-temperature maximum. Relative to dry B_2O_3, the activation energy corresponding to the high-temperature peak as increased by about 8.5 kJ/mol and the time constant has decreased to about one-third of the original value. The relative intensity of this peak, compared to the low-energy peak, appears to be smaller in the wet specimen.

Both the increased water vapor and oxygen partial pressure provide a source for an increased amount of oxygen in the melt, and would allow for the formation of nonbridging oxygens. The formation of singly bonded oxygens enhances the mobility of network components in the vicinity of the unsaturated BO_3 units. Acoustic phonons passing through such a defective region encounter a discontinuity which impedes the transmission of elastic strain energy. Instead, the energy is converted into a localized vibration of the partially connected BO_3 unit. Conversely, the reduction of the water vapor and oxygen partial pressures would increase the amount of bridging oxygens, hence strengthen the network and reduce the amount of mobile structural components. We already established that the humidity level has no effect on the low-temperature peak, neither does the oxygen partial pressure. When reducing the oxygen activity, neither the intensity of the low-activation energy dissipation mechanism nor the rate of decrease of the elastic modulus are changed. Consequently, the network degradation immediately above T_g does not seem to involve the formation of nonbridging oxygens.

Neither the formation of terminating hydroxyl groups nor the availability of excess oxygen affect the low-activation energy dissipation mechanism. These observations suggest that the initial network degradation occurs via simultaneous exchange of oxygens between adjacent B-O-B segments, so that two small rings are converted into one larger ring. A cartoon of this mechanism is shown in Fig. 8. In the displayed scenario, two boroxol rings approach each other such that a boron and an oxygen of one ring face an oxygen and a boron of the other one, respectively. Each boron, now coordinated by four oxygens, is lifted out of the plane containing the original three oxygens. Eventually, the lined-up boron-oxygen bonds are broken and immediately replaced with bonds between atoms in the adjacent planes. After the switch, the boron atom is still not contained in the plane formed by the new oxygen triangle. Structural relaxation is constrained by the connectivity in the surrounding network. While progressively increasing the ring sizes in the network, this mechanism does not produce nonbridging oxygens. However, as long as the overall network connectivity is large, i.e., immediately above T_g, this process requires the distortion of BO_3 units into nonplanar

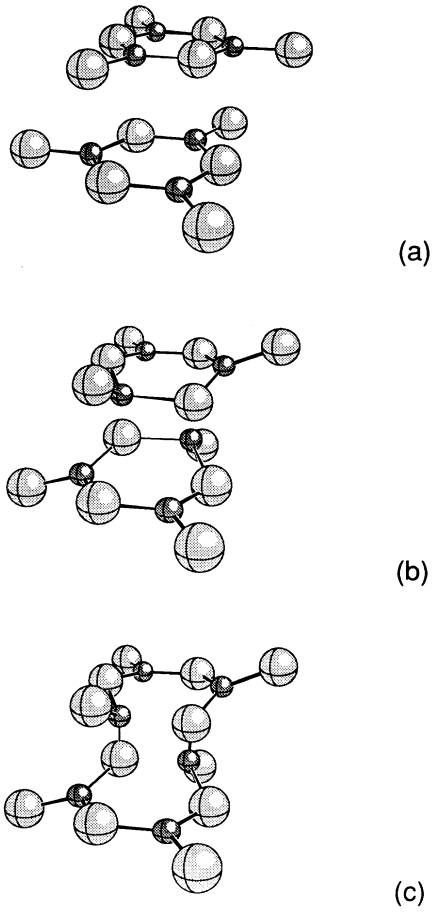

FIG. 8. Schematic of the depolymerization reaction in borates, occurring immediately above T_g. (a) Two boroxol rings positioned such that one oxygen and one boron of one ring respectively face a boron and an oxygen in the other ring. (b) The two BO_3 triangles distort into BO_4 tetrahedra, using one oxygen from the adjacent ring. (c) Two bonds originally within the boroxol rings break and two new bonds form between the rings.

configurations. This distortion can propagate via networked BO_3 units, and, due to long-range Coulomb forces, it can exchange energy between neighboring segments that are not directly connected. We propose that the momentum exchange associated with these nonplanar BO_3 distortions is at the origin of the low-energy dissipation maximum.

The proposed depolymerization mechanism is not only restricted to boroxol rings. It can invoke network structures of any size and shape, as long as an antisymmetric alignment of a B-O segment can be established. In binary borates the alkali oxide introduces additional oxygen, which is used for the formation of four coordinated borons. At alkali concentrations of less than 33 mol %, this additional oxygen is shared between two borons, and hence establishes additional crosslinking between neighboring planes of the boron-oxygen network. This crosslinking explains the increase in the room temperature elastic modulus of the binary alkali borates. Above T_g the rate with which the network disintegrates upon increasing temperature is higher than for pure boron oxide. In binary systems two mechanisms can contribute towards depolymerization: one is the same as described above, and the other one is the rupture of the crosslinks between planes. Both situations involve the deformation of BO_3 units, displacing borons back and forth between triangular and tetrahedral coordination by oxygen. This explains the match in activation energies for binary borates, as well as pure B_2O_3, since the mechanism associated with the initial network degradation is the same.

The relaxation mechanism characterized by the intermediate activation energy of approximately 45 kJ/mol can be attributed to the motion of alkali cations, since the amount of energy dissipated by this mechanism increases with increasing alkali concentration. We have shown this in more detail in a previous publication.[28] The high-activation energy mechanism becomes active when the borate network undergoes a final disintegration. At this stage oxygen anions form a more or less random structure, and boron cations can jump between sites. Upon increasing the alkali oxide content, the magnitudes of the activation energies for boron and alkali cation motion converge, indicating that both types of cations experience similar environments. As seen in Fig. 5, the effect of water is an increase in activation energy for the boron motion and a decrease in the amount of energy dissipated by this process. Apparently, the formation of OH terminal groups impedes the motion of boron, by restricting the number of available sites. Conversely, high nitrogen activities favor the boron mobility. Nitrogen can substitute oxygen as a network element, but offers a higher functionality. Hence, more sites become available for the borons.

VI. CONCLUSION

Using an expression for the dynamic structure factor based on the generalized hydrodynamic formalism, the line shapes of Brillouin spectra have been analyzed to yield the real and imaginary components of a complex mechanical modulus. This modulus describes the dynamic response of equilibrium structures on a molecular scale. It furnishes the zero-shear rate viscosity. Due to the high probing frequencies the light scattering probe is particularly sensitive to changes in the preexponential time constant. The storage modulus provides an excellent means for monitoring the structural developments upon changing the temperature. The dynamic viscosity derived from the Brillouin linewidths encompasses mechanisms of momentum transport which do not displace the system from thermal equilibrium, and by this virtue represent the zero-frequency limit of this coefficient. The activation energies and preexponential time constants describing the motion of structural components, leading from low- to high-temperature structures, are the same as those describing the loss of structural rigidity during this transition. The applicability of a simple mechanical relaxation formalism for the description of the glass-to-liquid transition suggests that thermal and mechanical energy invoke similar structural changes.

The transition from a room temperature borate glass to a high-temperature liquid involves relatively distinct mechanisms. While each mechanism may have a narrow spread of characteristic relaxation times, they remain fairly distinguishable in the temperature spectrum. These mechanisms include (i) the oscillation of boron between triangular and tetrahedral coordination by oxygen, eventually involving the exchange of one neighboring oxygen, (ii) the motion of alkali cations in between network segments, and (iii) the diffusive jumps of dissociated boron cations between oxygen interstices.

Neither the water nor the oxygen partial pressure, with which the samples were equilibrated, has an effect on the network degradation immediately above T_g. This finding suggests that the initial network depolymerization occurs predominantly via mutual exchange of one oxygen per BO_3 units, involving two units in adjacent network segments. This mechanism allows for a progressive increase of the network ring sizes without the formation of nonbridging oxygens. The molecular displacements involved in the associated structural relaxation are characterized by the lowest activation energy of all transition processes. Further network degradation occurs at higher temperature, where the identity of the oxygens coordinating a particular boron changes rapidly. The concept of a BO_3 network no longer applies. All cations, whether borons or alkalis, experience a similar oxygen environment and exhibit high mobilities. Under these conditions, the light scattering experiment and rotating cylinder viscometry yield viscosity data which are in close agreement.

ACKNOWLEDGMENTS

This work was supported by the National Science Foundation under Grant No. MSS 90-08918.

[1]R. L. Mozzi and B. E. Warren, J. Appl. Crystallogr. **3**, 251 (1970).
[2]F. L. Galeener, G. Lucovsky, and J. C. Mikkelsen, Jr., Phys. Rev. B **22**, 3983 (1980).
[3]G. E. Walrafen, M. S. Hokmabadi, P. N. Krishnan, and S. Guha, J. Chem. Phys. **79**, 3609 (1983).
[4]P. J. Bray, S. A. Feller, G. E. Jellison, Jr., and J. H. Yun, J. Non-Cryst. Solids **38-39**, 39 (1980).
[5]C. F. Windish, Jr. and W. M. Risen, Jr., J. Non-Cryst. Solids **48**, 307 (1982).
[6]J. Krogh-Moe, J. Non-Cryst. Solids **1**, 269 (1969).
[7]C. A. Angell, J. Non-Cryst. Solids **131-133**, 13 (1991).
[8]A. Napolitano, P. B. Macedo, and E. G. Hawkins, J. Am. Ceram. Soc. **48**, 613 (1965).
[9]R. E. Eppler, J. Am. Ceram. Soc. **49**, 679 (1966).
[10]G. H. Kaiura and J. M. Toguri, Phys. Chem. Glasses **17**, 62 (1976).
[11]G. Adams and J. H. Gibbs, J. Chem. Phys. **43**, 139 (1965).
[12]A. K. Hassan, L. M. Torell, L. Börjesson, and H. Doweidar, Phys. Rev. B **45**, 12 797 (1992).
[13]C. R. Kurkjian and J. T. Krause, J. Am. Ceram. Soc. **49**, 171 (1966).
[14]J. Tauke, T. A. Litovitz, and P. B. Macedo, J. Am. Ceram. Soc. **51**, 158 (1968).
[15]R. D. Mountain, J. Res. NBS **70A**, 207 (1966).
[16]D. A. McQuarrie, *Statstical Mechanics* (Harper and Row, New York, 1976).
[17]J. P. Boon and S. Yip, *Molecular Hydrodynamics* (Dover, New York, 1991).
[18]N. J. Tao, G. Li, and H. Z. Cummins, Phys. Rev. B **43**, 5815 (1991).
[19]W. Götze and M. Lücke, Phys. Rev. A **11**, 2173 (1975).
[20]J. Bosse, W. Götze, and M. Lücke, Phys. Rev. A **18**, 1176 (1978).
[21]W. Götze, in *Amorphous and Liquid Materials,* Vol. 118 of *NATO Advanced Study Institute, Series E: Applied Sciences,* edited by E. Lüscher, G. Fritsch, and G. Jacucci (Martinus Nijhoff, Dordrecht, 1987).
[22]K. F. Herzfeld and T. A. Litovitz, *Absorption and Dispersion of Ultrasonic Waves* (Academic, New York, 1959).
[23]J. R. Sandercock, in *Light Scattering in Solids III,* edited by M. Cardona and G. Güntherdt, Topics in Applied Physics Vol. 51 (Springer, Berlin, 1983), p. 173.
[24]O. Mazurin, *Handbook of Glass Data* (Elsevier, New York, 1987), Vol. C.
[25]J. Kieffer and J. B. Wagner, J. Electrochem. Soc. **135**, 198 (1988).
[26]J. E. Masnik, J. Kieffer, and J. D. Bass, J. Am. Ceram. Soc. **76**, 3073 (1993).
[27]J. T. Krause and C. R. Kurkjian, in *Borate Glasses: Structure, Properties, Applications,* edited by L. D. Pye, V. D. Frechette, and N. J. Kreidel (Plenum, New York, 1978), p. 577.
[28]J. Kieffer, J. E. Masnik, B. J. Reardon, and J. D. Bass, *Crystallization and Related Phenomena in Amorphous Materials—Ceramics, Metals, Polymers, and Semiconductors,* edited by M. Libera, T. E. Haynes, P. Cebe, and J. Dickinson, MRS Symposia Proceedings No. **321** (Materials Research Society, Pittsburgh, 1994).

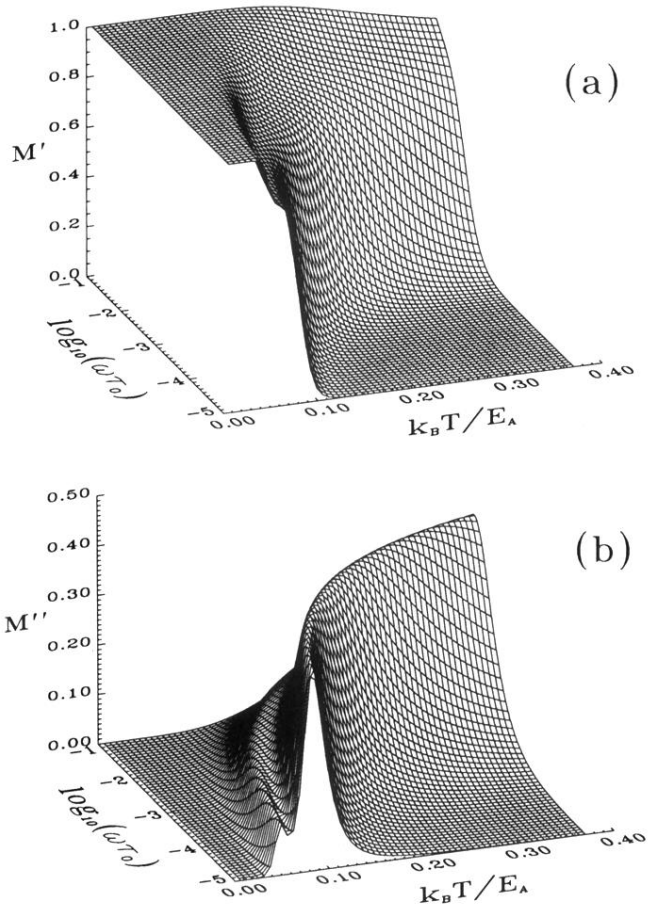

FIG. 1. (a) Schematic of the real component of the complex mechanical modulus, as a function of the normalized temperature, k_BT/E_A, where E_A is the activation energy of the relaxation process, and the normalized frequency, $\omega\tau_0$, where τ_0 is the time constant of the process. Two hypothetical mechanisms are superimposed. (b) Schematic of the imaginary component of the complex mechanical modulus, as a function of the normalized temperature, k_BT/E_A, where E_A is the activation energy of the relaxation process, and the normalized frequency, $\omega\tau_0$, where τ_0 is the time constant of the process. Two hypothetical mechanisms are superimposed.

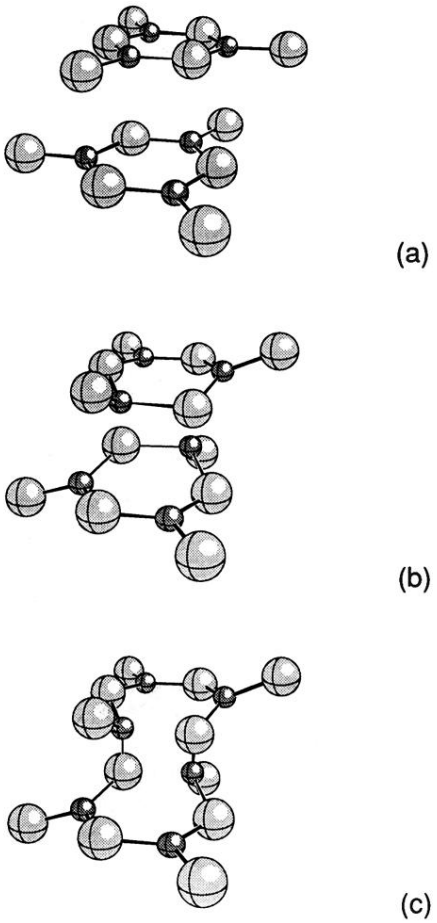

FIG. 8. Schematic of the depolymerization reaction in borates, occurring immediately above T_g. (a) Two boroxol rings positioned such that one oxygen and one boron of one ring respectively face a boron and an oxygen in the other ring. (b) The two BO_3 triangles distort into BO_4 tetrahedra, using one oxygen from the adjacent ring. (c) Two bonds originally within the boroxol rings break and two new bonds form between the rings.